Supplementary Information

Supplemental Methods

Mice. Mouse strains in a C57BL/6 background were housed in a pathogen-free facility in accordance with the INSERM guidelines. Mouse experiments were approved by the Institutional Animal Care and Use committee of the University of Nice Sophia-Antipolis (Nice, France), and performed with 8 to 12-week-old mice. Littermates were used as controls.

Generation and characterization of cherubic mice. Cherubic mice were generated by knocking-in the GGA to CGA mutation in *sh3bp2* exon 9, resulting in a Gly_{418} to Arg substitution in 3BP2 protein. The mouse mutation G418R is analogous to the G420R mutation frequently found in human cherubic patients (ref. (1)). The cherubic $sh3bp2^{G418R}$ mouse line was established at the ICS (Institut Clinique de la Souris, Illkirch, France; http://www.ics-mci.fr/). The targeting vector was constructed as follows. A 4.2 kb fragment encompassing exons 5 to 8 (5' homology arm) and a 3.2 kb fragment encompassing exon 13 (3' homology arm) were amplified by PCR from genomic DNA and subcloned in an ICS proprietary vector, resulting in step1 plasmid. This ICS vector has a floxed neomycin resistance cassette. A 1.5 kb fragment encompassing exon 9 was amplified by PCR and subcloned in step1 plasmid to generate the final targeting construct in which the GGA to CGA mutation in *sh3bp2* exon 9 was introduced (Supplemental Figure 5A). The linearized construct was

electroporated in 129S2/SvPas mouse embryonic stem (ES) cells. After selection, targeted clones were identified by PCR using external primers and further confirmed by Southern blot with 5' and 3' external probes (Supplemental Figure 5B). 4 positive ES clones were injected into C57BL/6J blastocysts, and male chimaeras derived gave germline transmission. WT, heterozygous (*sh3bp2*$^{WT/KI}$) and homozygous (*sh3bp2*$^{KI/KI}$) cherubic mice in a C57BL/6 background were housed in a pathogen-free facility. While heterozygous mice showed no significant abnormalities by visual inspection, homozygous presented swelling of facial soft tissues with eyelid closure starting about 6 weeks after birth (Supplemental Figure 6A). Radiographic analysis was performed on 4 month-old WT, heterozygous and homozygous cherubic mice using a FAXITRON system (Faxitron Bioptics, Tucson, USA). X-ray analysis revealed severe bone losses on the skull, ribs, vertebrae and legs of homozygous mice, but not WT and heterozygous mice (Supplemental Figure 6B, arrowheads). Homozygous mice specifically developed lymphadenopathy, monocytosis (Supplemental Figure 6, C and D), and spontaneous production of inflammatory cytokines (IL-6, IL-12p70 and TNF-[illegible]) in the serum (Supplemental Figure 6E). The $Gly_{418}Arg$ mutation introduced in the *sh3bp2* gene generated a cherubic phenotype that was similar to the one described in the $Pro_{416}Arg$ mutant mice generated by Ueki et al. (ref. (2)), thus validating our model. In addition, consistent with the study by Levaot et al. on osteoclasts from $Pro_{416}Arg$ cherubic mice (ref. (3)), immunoblot analysis showed that 3BP2 $Gly_{418}Arg$ mutant proteins progressively accumulated in

heterozygous (*sh3bp2*$^{WT/KI}$) and homozygous (*sh3bp2*$^{KI/KI}$) BMM (Supplemental Figure 6F).

In vivo LPS challenge. 1.8 mg/kg LPS (*E. coli* strain 055:B5, Sigma) was injected i.p.. Blood was harvested 4 h later by cardiac puncture and cytokines in the serum were measured by ELISA (eBioscience). In other experiments, 10 µg/ml LPS was added in drinking water of 5 weeks-old mice for 28 days. TNF-α was measured in the serum 3 days after LPS removal.

Antibiotics treatment. Four week-old mice were fed for 4 weeks with or without ampicillin (0.5 mg/ml), gentamicin (0.5 mg/ml), metronidazole (0.5 mg/ml), neomycin (0.5 mg/ml) and vancomycin (0.25 mg/ml) in autoclaved water. For optimal mouse hydration, we supplemented control and antibiotic water with 5% sucrose. Control and antibiotic water bottles were preserved from light and changed twice a week. Blood was then harvested by cardiac puncture and TNF-α was measured in the serum by ELISA.

Bacteremia assay. 10^7 *E. coli* (strain UTI-89) (4) were injected in mice tail vein. 10 µl of blood were harvested from mice tails 3, 6, 24 and 48 h after injection and plated on LB-agar with antibiotics. After overnight incubation at 37°C, *E. coli* colonies were counted.

Peritoneal macrophage adoptive transfer. To generate peritoneal macrophages, 1 ml

thioglycolate (TG) brewer 4% (Sigma) was injected i.p. in donor WT and 3BP2-deficient mice. 5 d later, 7 ml of ice-cold 30% sucrose solution was injected into peritoneal cavity of euthanized mice and aspirated back. Peritoneal cells were washed in cold PBS, stained for 15 min with 10 µM CFSE (Life Technologies), incubated for 30 min at 37°C in warmed PBS to discard excess CFSE, and 10^7 cells were harvested in 200 µl PBS for injection in the tail vein of WT recipient mice. 2 d before receiving TG-elicited peritoneal macrophages, recipient mice were injected with 200 µl clodronate liposomes i.p. to deplete intrinsic macrophages. 16 h after cell injection, recipient mice were challenged with LPS as described above. Spleens from recipient mice were harvested at the end of the experiment to check intrinsic macrophage depletion and CFSE-labeled macrophage colonization by flow cytometry.

Flow cytometry. FACS acquisition was performed with a BD FACSCanto™ II flow cytometer (BD Biosciences) and analyzed with the BD FACSDiva™ software. mAb used were: mouse anti CD83-APC (BD Pharmingen), CD16/32-FITC and CD206-Alexa Fluor® 488 (BioLegend), MARCO-FITC (AbD Serotec), CD11b-PerCP-Cy5.5, CD14-FITC, CD80-PE, CD86-PE, DECTIN1-PE, F4/80-APC-eFluor780, MHC II (I-A/I-E)-APC, NOS2-PE, TLR4-PE-Cy7 and TLR9-FITC (eBioscience). Macrophages were gated as $CD11b^+$ / $F4/80^+$ cells.

BM-derived DC cultures. BM cells from mice tibias and femurs were flushed out with ice-cold PBS containing 2% FBS and 2 mM EDTA. Cell suspension was filtered through a 70 mm nylon cell strainer and red blood cells were lysed with red blood cell

lysis buffer (Sigma). Cells were then cultured for 7 d with RPMI-1640 with 10% FBS, 50 U/l penicillin, 50 µg/l streptomycin, 1 mM sodium pyruvate, 10 µM HEPES, MEM Non-Essential Amino Acids 1X and 50 µM 2-mercaptoethanol containing 10 ng/ml IL-4 and 10 ng/ml GM-CSF (eBioscience) in 6-well plates.

Osteoclast differentiation and TRAP staining. $5x10^4$ BM $^{cells}/cm^2$ were cultured in the presence of 50 ng/ml M-CSF (eBioscience) and 100 ng/ml RANKL (R&D Systems) for 1 to 5 d at 37°C in 5% CO2. The culture medium was changed at day 3. Tartrate resistant acid phosphatase (TRAP) staining was performed using the Leukocyte acid phosphatase kit (Sigma-Aldrich) according to the manufacturer's protocol and as described before (5). The number of $TRAP^+$ cells per well and the number of nuclei per $TRAP^+$ cell was then counted and scored by microscopy on 6 independent fields.

F-actin staining of osteoclasts. Osteoclasts cultured onto chamber slide were fixed, permeabilized and incubated with 100 ng/ml of Alexa Fluor 594 phalloidin and 500 nM DAPI (Life Technologies) at 22°C in a humidified atmosphere for 30 min. After staining, cells were washed with PBS, rinsed with water and mounted with Fluoromount (Sigma). Polymerized actin was visualized using a Zeiss Axiovert 200M fluorescence microscope equipped by a Hamamatsu ORCA-ER digital camera (Hamamatsu). Image analysis was performed with Volocity software (Improvision Inc.).

Real-time quantitative PCR. Total RNA from osteoclasts were reverse transcribed using the High Capacity cDNA Archive random priming Kit (Applied Biosystems). Real-time quantitative PCR (qRT-PCR) was performed using a 7900HT Sequence Detector System (Applied Biosystems) and the SYBR Green dye detection protocol as previously described (9). Relative expression level of target genes mRNA between control (X) and sample (Y) was calculated using the formula ΔC_T Y − ΔC_T X and expressed as fold over control ($2\Delta\Delta C_T$).

Supplemental Bibliography

1. Reichenberger EJ, Levine MA, Olsen BR, Papadaki ME, and Lietman SA. The role of SH3BP2 in the pathophysiology of cherubism. *Orphanet J Rare Dis.* 2012;7 Suppl 1(S5.
2. Ueki Y, Lin CY, Senoo M, Ebihara T, Agata N, Onji M, Saheki Y, Kawai T, Mukherjee PM, Reichenberger E, et al. Increased myeloid cell responses to M-CSF and RANKL cause bone loss and inflammation in SH3BP2 "cherubism" mice. *Cell.* 2007;128(1):71-83.
3. Levaot N, Voytyuk O, Dimitriou I, Sircoulomb F, Chandrakumar A, Deckert M, Krzyzanowski PM, Scotter A, Gu S, Janmohamed S, et al. Loss of Tankyrase-mediated destruction of 3BP2 is the underlying pathogenic mechanism of cherubism. *Cell.* 2011;147(6):1324-39.
4. Chen SL, Hung CS, Xu J, Reigstad CS, Magrini V, Sabo A, Blasiar D, Bieri T, Meyer RR, Ozersky P, et al. Identification of genes subject to positive selection in uropathogenic strains of Escherichia coli: a comparative genomics approach. *Proc Natl Acad Sci U S A.* 2006;103(15):5977-82.
5. GuezGuez A, Prod'homme V, Mouska X, Baudot A, Blin-Wakkach C, Rottapel R, and Deckert M. 3BP2 Adapter protein is required for receptor

activator of NFkappaB ligand (RANKL)-induced osteoclast differentiation of RAW264.7 cells. *J Biol Chem.* 2010;285(27):20952-63.

Supplemental Figure Legends

Supplemental Figure 1: Number and phenotype of monocytes and macrophages in WT, 3BP2-deficient and cherubic mice. (A) Monocyte number and **(B)** phenotype in the blood of mice (n=6). **(C)** Macrophage number and **(D)** phenotype in the spleen of mice (n=5). **(E)** TLR4 and TLR9 expression on BMM was analyzed by flow cytometry (n=3). Expression of M1/M2 markers of macrophage differentiation analyzed by **(F)** flow cytometry on spleen macrophages (n=3) or **(G)** by qRT-PCR on BMM (n=2, in triplicate).

Supplemental Figure 2: Peritoneal recruitment of macrophages is unaffected in 3BP2-deficient mice. (A) Number and **(B)** percentage of macrophages in the mice peritoneal cavity 3 h after LPS i.p. injection (n=3). (**C)** Number of peritoneal macrophages 5 days after i.p. injection of thioglycolate (n=9).

Supplemental Figure 3: Macrophages from 3BP2-deficient mice display impaired cytokine response to PAMP challenge. WT recipient mice were depleted from $CD11b^{+}/F4/80^{+}$ intrinsic macrophages following i.p. injection of clodronate liposomes **(A)**, and injected with WT and $sh3bp2^{KO/KO}$ thioglycolate-elicited peritoneal macrophages **(B)**. 24 h later, mice were injected i.p. with LPS and cytokines in the serum were measured by ELISA 4 h later (**C)**. Kinetics studies of BMM from WT or $sh3bp2^{KO/KO}$ mice stimulated with LPS **(D)** or CpG ODN **(E)**. **(F)** Dose response study of BMM from WT or $sh3bp2^{KO/KO}$ mice stimulated with LPS. TNF-α was measured in the supernatant by ELISA (***$P < 0.001$; **$P < 0.01$; *$P < 0.05$).

Supplemental Figure 4: Differentiation and function of 3BP2-deficient DC are unaffected. (A) Expression of 3BP2 in macrophages and DC derived from WT and 3BP2-deficient BM cells incubated respectively with M-CSF or GM-CSF + IL-4. ERK2 expression was used as a loading control. **(B)** BM-DC from WT and 3BP2-deficient mice were stimulated with LPS for 16 h. IL-12p70 in the supernatant was measured by ELISA (n=3).

Supplemental Figure 5: Generation of the $sh3bp2^{G418R}$ cherubic mouse. (A)

Strategy for the generation of a $Gly_{418}Arg$ mutation in *sh3bp2* by introducing the GGA to CGA mutation in exon 9 of *sh3bp2* gene, and **(B)** excision of the neomycin (Neo) selection marker.

Supplemental Figure 6: Phenotypic characterization of the *sh3bp2*^{G418R} (*sh3bp2*^{KI}) cherubic mouse. (A) Pictures of 10 weeks-old mice with *sh3bp2*$^{KI/KI}$ mice showing characteristic closed eyelids. **(B)** Radiographic analysis of 12 week-old mice with *sh3bp2*$^{KI/KI}$ mice showing multiple zones of bone loss (arrowhead). **(C)** Enlarged lymph nodes, and **(D)** bone marrow monocytosis of *sh3bp2*$^{KI/KI}$ mice (n=3). **(E)** Cytokines in the serum of *sh3bp2*$^{WT/WT}$, *sh3bp2*$^{WT/KI}$ and *sh3bp2*$^{KI/KI}$ were measured by ELISA (n=3). **(F)** Immunoblot analysis of 3BP2 expression in lysates from *sh3bp2*$^{WT/WT}$, *sh3bp2*$^{WT/KI}$ and *sh3bp2*$^{KI/KI}$ BMM. HSP60 expression was used as a loading control. Sensitivity of mice to septic choc was analysed by **(G)** bacteriemia (n=14) and **(H)** survival assays (n=14) (***$P < 0.001$; **$P < 0.01$; *$P < 0.05$).

Supplemental Figure 7: Reduced LPS-induced actin polymerization in 3BP2-deficient peritoneal macrophages, but not in 3BP2-deficient DC. (A) Morphology of WT and 3BP2-deficient BMM. Polymerized actin was visualized following Alexa Fluor® 488 phalloidin staining using a Zeiss Axiovert fluorescence microscope. Image analysis was performed with Volocity software. **(B)** Thioglycolate-elicited peritoneal macrophages were stimulated with LPS (1 μg/ml) for 10, 30 and 60 min at

37°C. Following fixation and permeabilization, cells were stained with Alexa Fluor 488® phalloidin and analyzed by flow cytometry. % actin polymerisation = (MFI sample with LPS/ MFI sample without LPS)*100. **(C)** BM-DC from WT and 3BP2-deficient mice were stimulated with LPS for 5, 10 or 30 min, stained with Alexa Fluor 488® phalloidin and analyzed by flow cytometry (*$P < 0.05$).

Supplemental Figure 8: BMM from 3BP2-deficient mice display impaired capacities to form osteoclasts *in vitro*. BMM from WT and 3BP2-deficient mice were cultured in the presence of M-CSF (50 ng/ml) and RANKL (40 ng/ml) for 1 to 7 days. **(A)** Representative micrographs of multinucleated cells either assayed for TRAP activity (upper panels) or labeled with Alexa Fluor 594® phalloidin and DAPI and analyzed by fluorescence microscopy (lower panels). **(B)** Quantification of $TRAP^+$ multinucleated cells and of the number of nuclei per osteoclast in wells obtained as in (A) (n=3). **(C)** Expression of osteoclastogenesis marker genes measured by qRT-PCR. Data represent the mean of mRNA relative expression of osteoclasts obtained at day 1 (d1), day 3 (d3) and day 7 (d7) after addition of M-CSF and RANKL.

Supplemental Figure 9: Effect of commensal microbiota depletion on systemic TNF-α production by cherubic heterozygous and homozygous mice. $sh3bp2^{WT/WT}$, $sh3bp2^{WT/KI}$ and $sh3bp2^{KI/KI}$ 4 week-old mice were treated with antibiotics in drinking water for 4 weeks (n=6). TNF-α was then measured in mice serum by ELISA (***$P < 0.001$; **$P < 0.01$).

Supplemental Figure 1

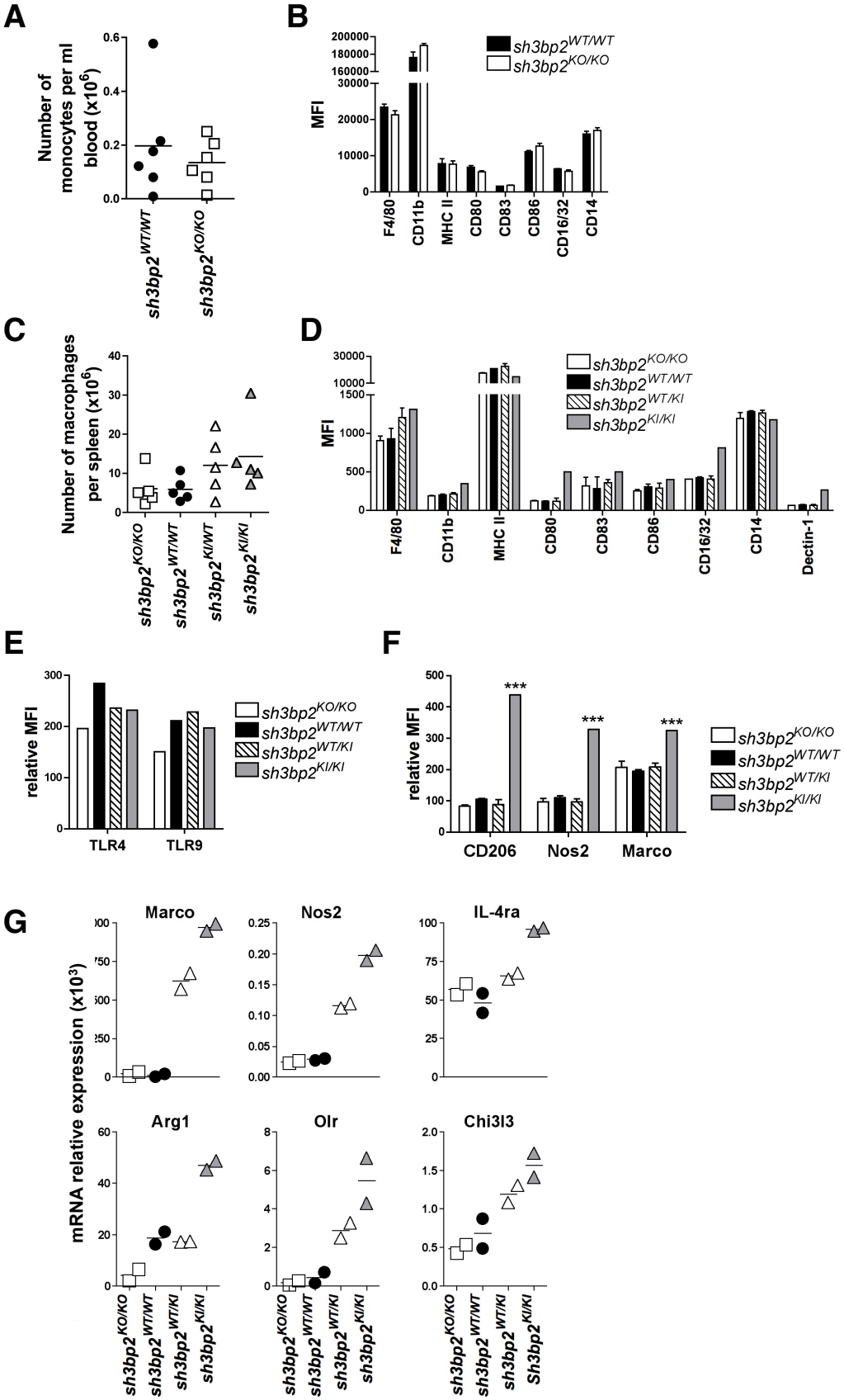

Supplemental Figure 2

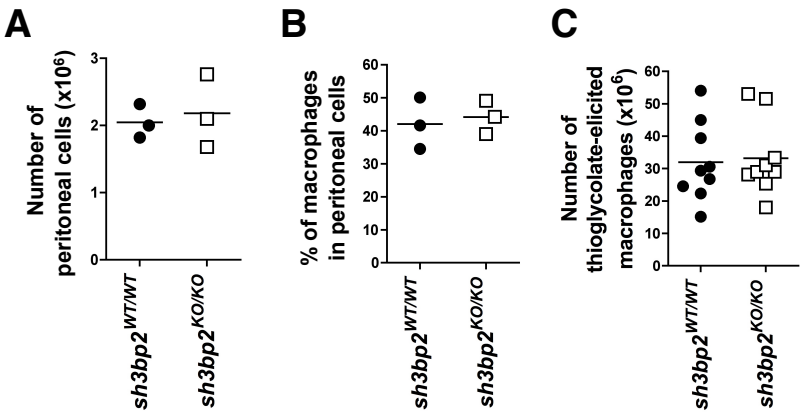

Figure S3

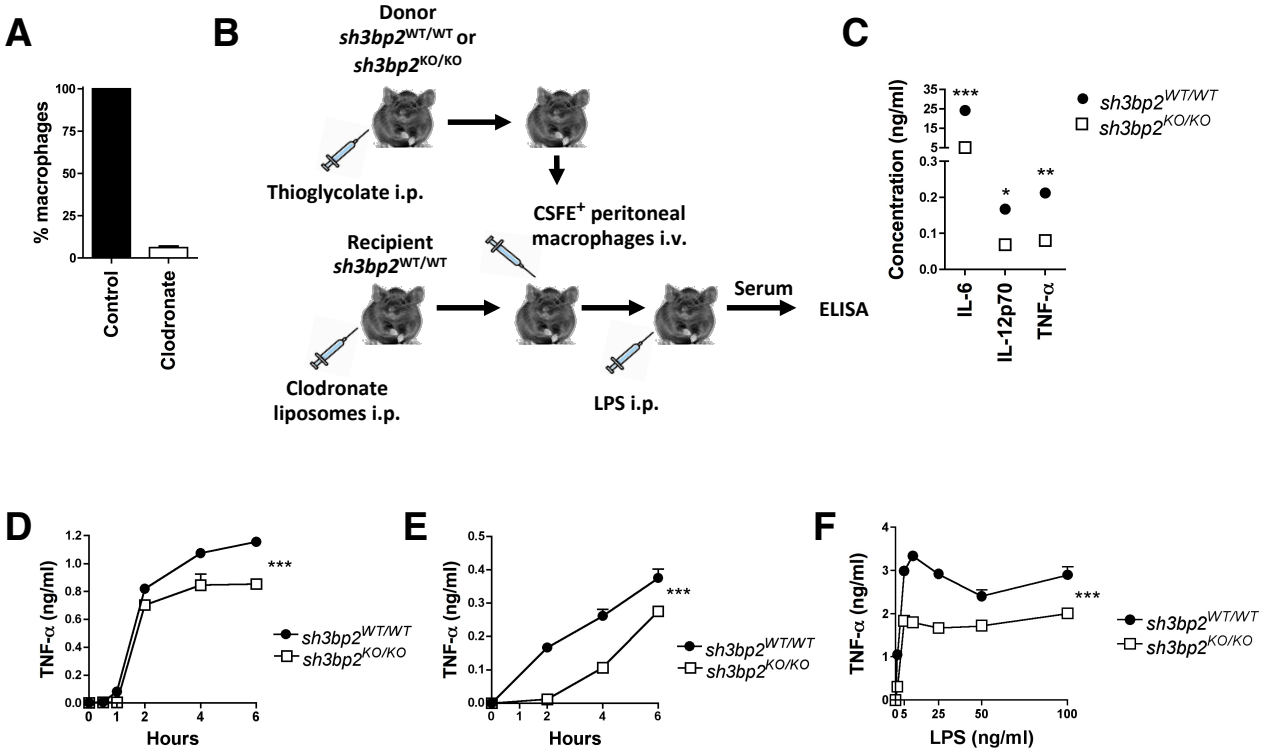

Supplemental Figure 4

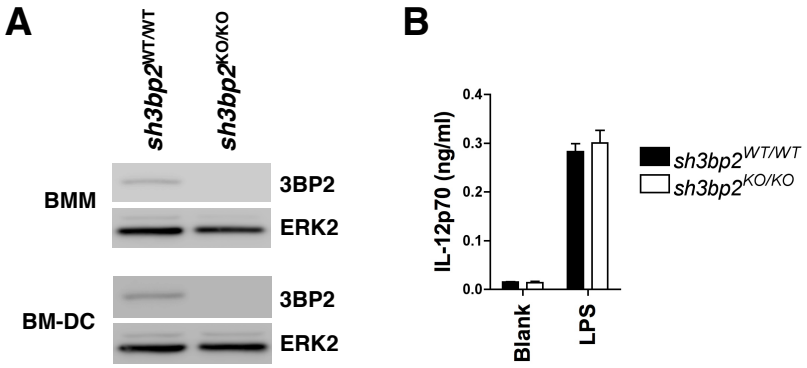

Supplemental Figure 5

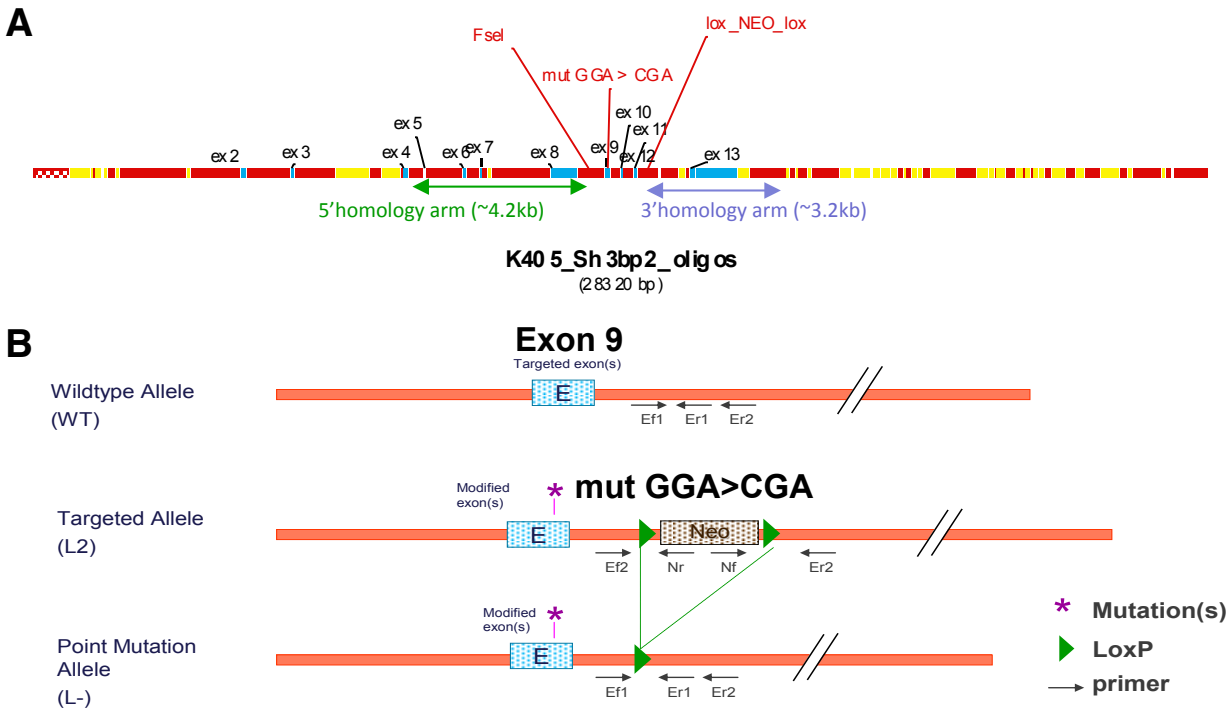

Supplemental Figure 6

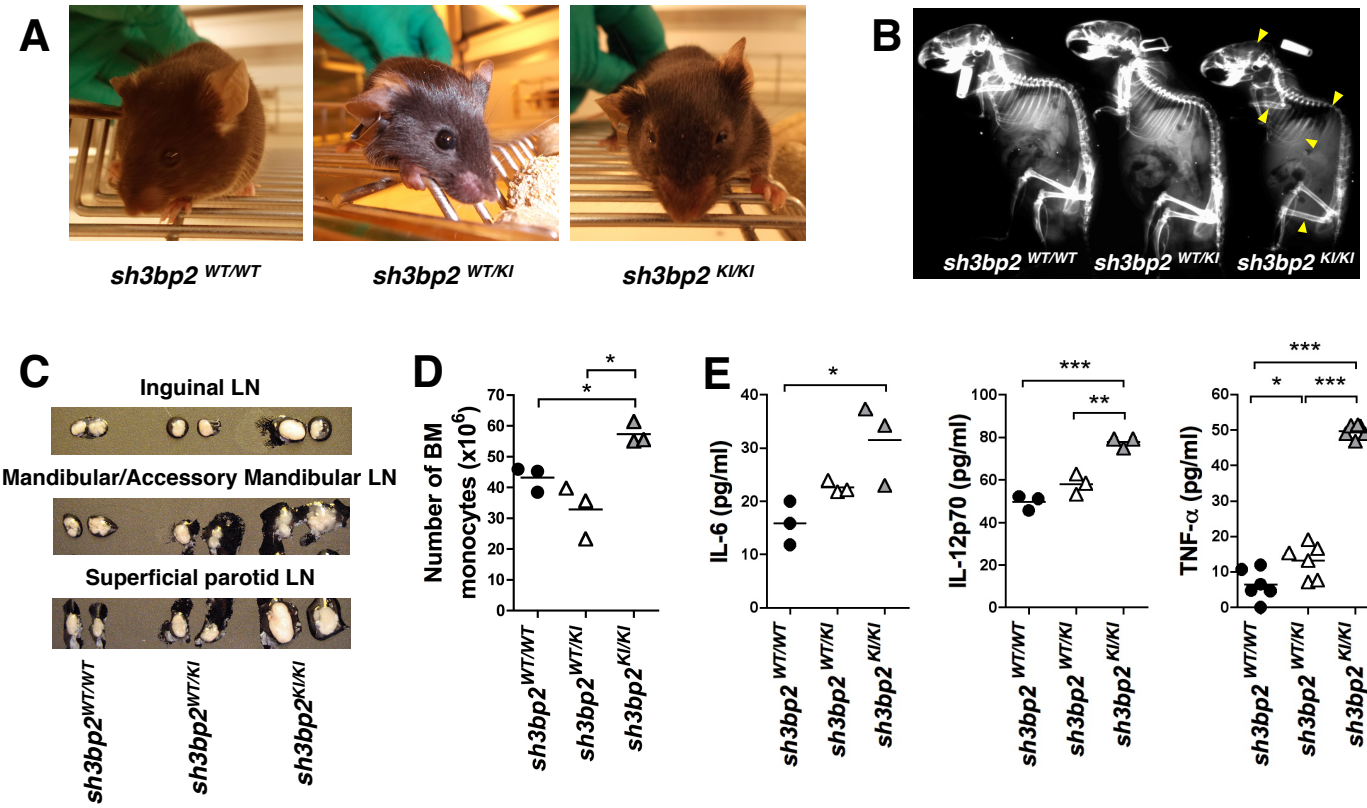

Supplemental Figure 7

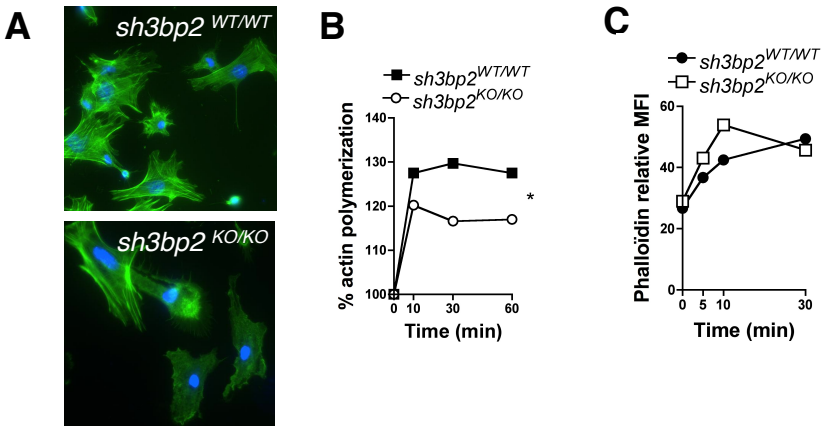

Figure S8

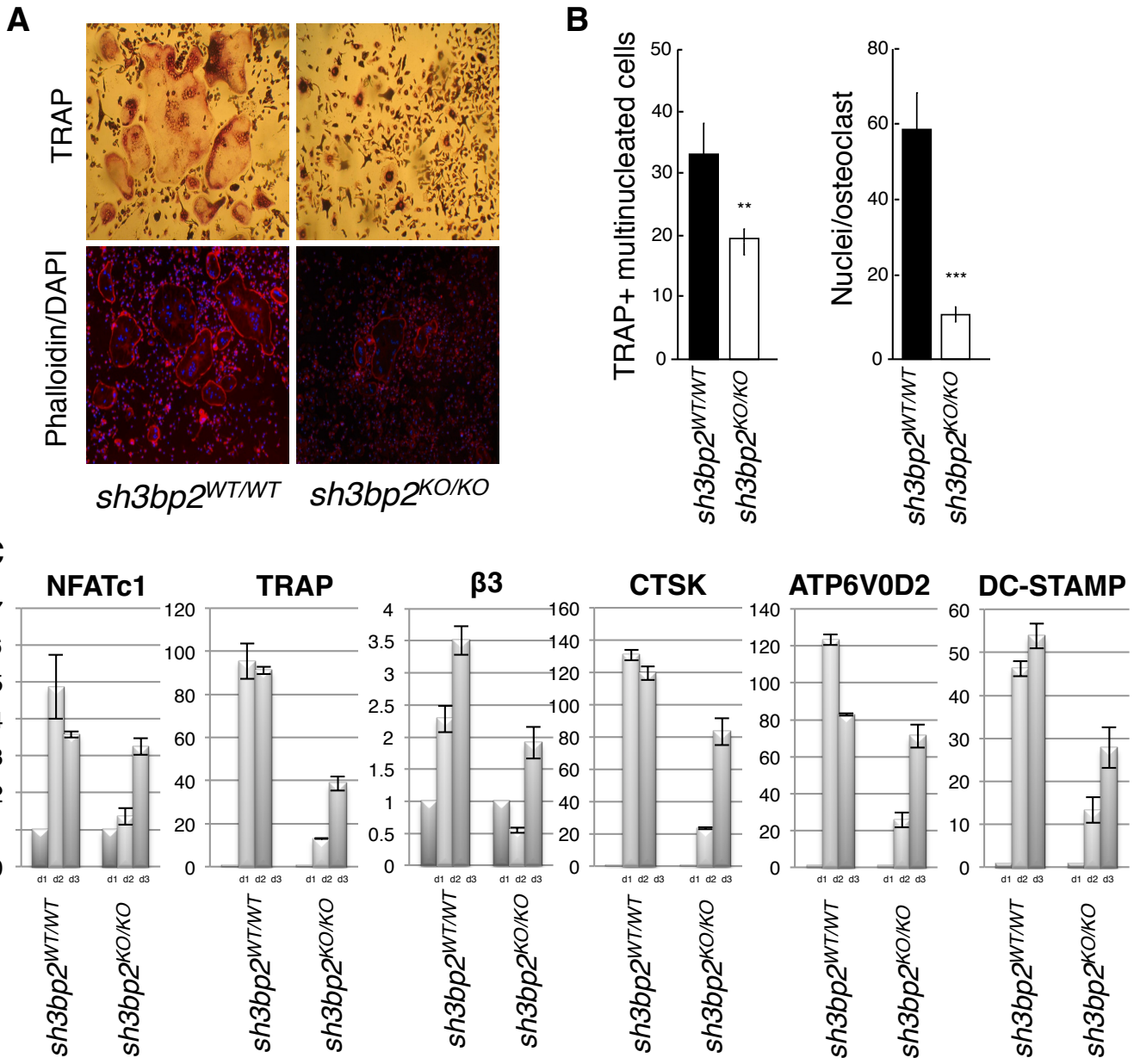
A
TRAP
Phalloidin/DAPI
sh3bp2WT/WT
sh3bp2KO/KO
B
TRAP+ multinucleated cells
Nuclei/osteoclast
**
***
C
mRNA relative expression
NFATc1
TRAP
β3
CTSK
ATP6V0D2
DC-STAMP
d1 d2 d3

Supplemental Figure 9